The Journal of Chemical Physics

Fast dynamics of a hydrogen-bonding glass forming liquid: Chemical exchange-induced spectral diffusion in 2D IR spectroscopy

Cite as: J. Chem. Phys. **150**, 124507 (2019); https://doi.org/10.1063/1.5088499
Submitted: 10 January 2019 . Accepted: 06 March 2019 . Published Online: 27 March 2019

David J. Hoffman, Sebastian M. Fica-Contreras, and Michael D. Fayer

COLLECTIONS

This paper was selected as an Editor's Pick

View Online Export Citation CrossMark

ARTICLES YOU MAY BE INTERESTED IN

Nucleation in aqueous NaCl solutions shifts from 1-step to 2-step mechanism on crossing the spinodal
The Journal of Chemical Physics **150**, 124502 (2019); https://doi.org/10.1063/1.5084248

An extension of the fewest switches surface hopping algorithm to complex Hamiltonians and photophysics in magnetic fields: Berry curvature and "magnetic" forces
The Journal of Chemical Physics **150**, 124101 (2019); https://doi.org/10.1063/1.5088770

Theory of coherent two-dimensional vibrational spectroscopy
The Journal of Chemical Physics **150**, 100901 (2019); https://doi.org/10.1063/1.5083966

© 2019 Author(s).

The Journal of Chemical Physics ARTICLE scitation.org/journal/jcp

Fast dynamics of a hydrogen-bonding glass forming liquid: Chemical exchange-induced spectral diffusion in 2D IR spectroscopy

Cite as: J. Chem. Phys. 150, 124507 (2019); doi: 10.1063/1.5088499
Submitted: 10 January 2019 • Accepted: 6 March 2019 •
Published Online: 27 March 2019

View Online Export Citation CrossMark

David J. Hoffman, Sebastian M. Fica-Contreras, and Michael D. Fayer[a)]

AFFILIATIONS

Department of Chemistry, Stanford University, Stanford, California 94305, USA

[a)]Email: fayer@stanford.edu. Telephone: 650 723-4446

ABSTRACT

Polarization-selective Two Dimensional Infrared (2D IR) and IR pump-probe spectroscopies have been performed on the hydrogen bonding glass forming liquid 2-biphenylmethanol doped with the long-lived vibrational probe phenylselenocyanate over a wide range of temperatures. The spectral diffusion seen in the 2D spectra was found to have a large polarization dependence, in large excess of what is predicted by standard theory. This anomaly was explained by decomposing the 2D spectra into hydrogen-bonding and non-bonding components, which exchange through large-angle orientational motion. By adapting chemical exchange theories, parameters for the component peaks were then calculated by fitting the polarization-dependent spectral diffusion and the pump-probe anisotropy. A model of highly heterogeneous exchange and orientational dynamics was used to explain the observed time dependences as a function of temperature on fast time scales. The experimental observations, the kinetic modeling, and physical arguments lead to the determination of the times for interconversion of slow dynamics structural domains to fast dynamics structural domains in the supercooled liquid as a function of temperature. The slow to fast domain interconversion times range from 40 ps at 355 K to 5000 ps at 270 K.

Published under license by AIP Publishing. https://doi.org/10.1063/1.5088499

I. INTRODUCTION

The polarization dependence of nonlinear spectra has long been used to obtain information on both structure and dynamics from a chemical system. In ultrafast infrared spectroscopy, polarization selective pump-probe experiments are a well-established method for measuring orientational relaxation.[1–4] In two-dimensional infrared (2D IR) spectroscopy, polarization experiments have been used to examine the angles between coupled dipoles,[5,6] the jump angle in a chemical exchange experiment,[7,8] to enhance cross peaks for molecular structure determination,[9,10] and recently to examine the impact of the orientational relaxation of a probe molecule on its spectral diffusion dynamics.[11–14] This last phenomenon, called reorientation-induced spectral diffusion (RISD), is particularly interesting as it provides additional information about the coupling between the instantaneous frequency of the probe and its environment.

2D IR spectroscopy can provide information on the ultrafast structural dynamics of a chemical system through the measurement of spectral diffusion of a vibrational probe.[15–17] The 2D IR experiment effectively labels the instantaneous vibrational frequencies of the vibrational probes at time zero (ω_1), allows the chemical system (and the corresponding instantaneous frequencies of the probes) to evolve for a known waiting time T_w, and then reads out the final frequencies of the probes (ω_3). For a T_w short compared to the dynamics of the system, the 2D line shapes will be highly correlated, i.e., elongated along the (ω_1, ω_3) diagonal, while at a long T_w, the line shapes will become decorrelated and round. The T_w dependent decorrelation (spectral diffusion) is quantified by the frequency-frequency correlation function (FFCF).

If RISD occurs, a component spectral diffusion is caused by the reorientational motion of the probe if there are significant directional interactions between the probe and environment, e.g., via a slowly time varying electric field interaction through the vibrational stark effect.[11] RISD is, in addition to spectral diffusion, caused by the structural evolution of the medium, i.e., structural spectral diffusion (SSD). RISD is manifested as a different extent of spectral diffusion for different polarizations of light in the 2D IR pulse sequence. By

Published under license by AIP Publishing

comparing the differences between the spectral diffusion observed with all four pulses (three input pulses and the echo pulse) having the same polarizations (parallel ⟨XXXX⟩) and the first two pulses having one polarization and the third pulse and the echo having perpendicular polarization (perpendicular ⟨XXYY⟩) and using the time dependence of the reorientation of the probe, determined with pump-probe anisotropy measurements, the components of the spectral diffusion can be separated into RISD and SSD. This approach of separating RISD contributions from the SSD has worked with excellent to a reasonable degree of success in a number of systems,[12,13,18] provided that the reorientation of the molecule does not significantly disturb the structure of the surrounding medium.

Besides local electric fields, an important, strongly directional interaction that commonly appears in chemical systems is hydrogen bonding. Hydrogen bonding (H-bonding) is often a significant feature of many molecular systems. H-bonding can occur among molecules in a pure liquid as well as between a liquid or a glass and a solute. In 2D IR experiments, the vibrational probe solute can H-bond to the solvent and provide details of H-bond interactions and dynamics.[19–21] While spectral diffusion polarization effects do not occur in water because it rapidly rearranges its H-bond network,[12,19] it is reasonable to expect other H-bonding systems to exhibit enhanced RISD-like behavior because of the strength and directionality of H-bonds.

In the following, we present polarization selective 2D IR experiments on the H-bonding glass forming liquid 2-biphenylmethanol (2BPM, see the structure in Fig. 1, inset). Glass formers are notable for having dynamics that are largely universal across a wide range of different types of intermolecular interactions and chemical species,[22–24] which make them useful for distinguishing the manner in which varying intermolecular interactions influence a given conserved dynamical process. In addition, relatively mild changes in temperature can substantially change the time scale on which a given dynamical process occurs. The behavior of solute molecules in H-bonding glassy systems is also important for a number of practical applications, ranging from the widespread use of carbohydrate glasses to preserve biological molecules[25] to the use of small plasticizers to tune the mechanical and thermodynamic properties of polyvinyl alcohol,[26] polyamides,[27,28] and cellulose-derived polymers.[29,30]

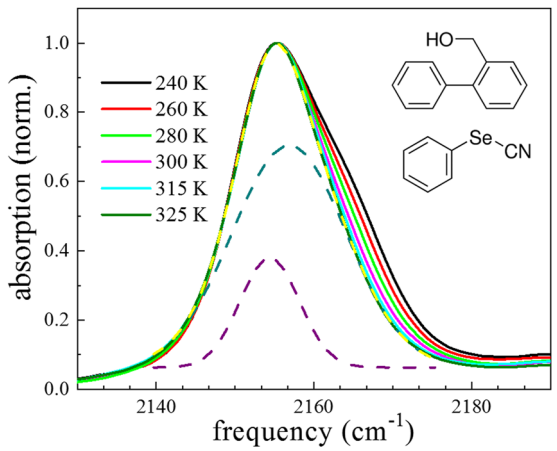

FIG. 1. Temperature dependent FT-IR spectra of the CN stretch of PhSeCN in 2BPM (structures depicted at top right). As the temperature is lowered, a blue wing grows on the spectra, consistent with the formation of stronger H-bonds. The yellow dashed curve is a fit to the 325 K spectrum with the sum of two Gaussians (smaller dashed curves). The smaller component Gaussian (violet dashed curve) has a similar spectrum as PhSeCN in non-H-bonding media.

Although the molecular glass former 2BPM has not been extensively studied, its dynamics have been previously observed with optical Kerr effect (OKE) spectroscopy[31,32] and its thermodynamics and structures have been examined with DSC, FT-IR, x-ray crystallography, and luminescence spectroscopy.[33–36] It also has structural similarities, a similar glass transition temperature (T_g), and similar thermodynamics in its slow "α-relaxation" as notable non-H-bonding molecular glass formers benzophenone (BZP) and *ortho*-terphenyl (OTP),[31,32] both of which have been studied using 2D IR spectroscopy.[37,38] Comparisons to non-H-bonding systems permit the examination of the impact of the H-bonding on structural dynamics and solute-solvent interactions.

To examine a wide range of time scales, the long-lived vibrational probe solute, phenylselenocyanate (PhSeCN, see the structure in Fig. 1, inset), was used. Selenocyanates are remarkable vibrational probes as their nitrile stretches have vibrational lifetimes on the order of hundreds of picoseconds,[39] which is two orders of magnitude longer than most vibrations, enabling the collection of IR pump-probe and 2D IR data from a few hundred femtoseconds to a nanosecond.[37,38]

The 2D IR experiments on 2BPM reveal that the observed spectral diffusion is substantially influenced by polarization. Polarization effects were previously found to be small to non-existent in 2D IR experiments on the structurally similar, dipolar glass forming liquid benzophenone (BZP).[38] Using the measured reorientational dynamics of PhSeCN, the standard RISD theory dramatically fails to describe the observations. The results demonstrate that H-bonding to the nitrile of PhSeCN is a significant contributor to the observed differences between 2D IR experiments on 2BPM and non-H-bonding liquids such as BZP.

Using temperature dependent FT-IR spectra and the frequency dependence of the vibrational lifetime, it was possible to decompose the 2D spectra into spectrally overlapped H-bonding and non-H-bonding components. The non-H-bonding component was found to have a very similar spectral width and vibrational lifetime as the PhSeCN vibrational probe in a non-H-bonding liquid,[38] while the H-bonding component of the spectrum was much broader and had a shorter vibrational lifetime, consistent with the behaviors of other H-bonded vibrational probes.[40] A model was developed in terms of chemical exchange between species with two heavily overlapped spectral bands. Using a model with a large change in orientation accompanying chemical exchange (a large jump angle), as has been observed in chemical exchange studies of water/ion solutions,[7,8] it was possible to calculate the 2D spectra that exhibited the same spectral diffusion as the experimental data.

While the model of exchange-induced spectral diffusion (XISD) proved capable of describing the data at early and late T_w's, there was still a noticeable systematic discrepancy at intermediate T_w's. The disparities at intermediate T_w's could be accounted for by a fast orientational process that both decorrelates the

Published under license by AIP Publishing

instantaneous frequencies of the probe molecules and creates separate populations that give rise to differences in the parallel and perpendicular decay curves. The pump-probe anisotropy decays are biexponential at all temperatures. By assuming that the observed nonexponential decays arise from differing rates of complete reorientation, the full range of data at all temperatures can be described well. From the experimental data and arguments from the associated thermodynamic trends, the exchange time between dynamically "fast" and "slow" domains was determined as a function of temperature.

The temperature dependence of 2BPM displays deviations from typical α-like relaxation, in contrast to prior dynamical measurements with OKE.[31,32] Both the slow exchange rate dynamics and the structural spectral diffusion approximately followed Arrhenius behavior from well above the melting point through 270 K, ~30 K above T_g, below which the slow dynamics became too slow to be measured within the experimental time window set by the vibrational lifetime. By contrast, the OKE measurements of the dynamics of 2BPM show that the slow relaxation becomes super-Arrhenius by 290 K.[31,32] The Arrhenius behavior of 2BPM is also in contrast to the dynamics measured for the non-H-bonding liquids BZP and OTP by both 2D IR[38] and OKE,[31,32] where the slow dynamics in both followed the same, super-Arrhenius temperature dependences.

II. EXPERIMENTAL METHODS AND RESULTS

A. Sample preparation and calorimetry

5 mol. % mixtures of PhSeCN (Sigma-Aldrich) and 2BPM (Sigma-Aldrich) were prepared and used without further purification. Differential scanning calorimetry measurements (Q2000 DSC at a 10 K/min ramp rate) gave a glass transition temperature T_g of the solution at ~236 K, several degrees below the T_g of the neat BPM liquid (~241 K). This is comparable to the shift in T_g seen in other liquids with similar concentrations of PhSeCN.[38]

For IR experiments, the solution was heated to approximately 50 °C and loaded between two 3 mm CaF_2 windows separated by a 190 μm Teflon spacer. The sample was placed in a copper cell, which was temperature controlled from 270 K to 355 K, ±0.05 K, using a Peltier thermoelectric device (TETechnology). At deep supercooling (<290 K), 2BPM showed an enhanced tendency to crystallize, requiring the sample to be reheated above its melting point and cooled again. This cycling limits the temperature stability to ±0.5 K for the lowest temperatures.

B. FT-IR spectroscopy

FT-IR experiments were performed with 1 cm^{-1} resolution. The spectra taken of neat 2BPM were subtracted from the PhSeCN solution to isolate the nitrile stretch of PhSeCN at ~2155 cm^{-1} to remove the already minimal background absorption. The spectra were obtained over a range of temperatures from 355 K to 270 K. Representative spectra are shown in Fig. 1.

At all temperatures, it is apparent that the spectra's full width at half maximum (FWHM), >13 cm^{-1}, is much larger than previously observed for PhSeCN in non-H-bonding liquids, ~8 cm^{-1}.[38] This significant broadening is characteristic of H-bonding in general and nitriles, in particular.[41] Furthermore, the FWHM in 2BPM is seen to be highly temperature dependent, again unlike the observation of the non-H-bonding liquids. As the temperature is lowered, a blue wing grows while the frequency of the maximum remains constant. This is consistent with the formation of stronger H-bonds at lower temperatures, which results in a blue shift for nitriles.[41–43] An analogous temperature dependence of the H-bonding of the neat liquid has been reported in the OH stretching region of FT-IR spectra.[33]

In addition to being much wider than in the non-H-bonding liquids, the nitrile peak in 2BPM is clearly asymmetrical. The spectrum for a given temperature can be fit very well using a sum of two Gaussian components: a small, narrow one at about 2154 cm^{-1} and a broader one at a slightly bluer, temperature dependent center frequency. The yellow dashed line is a fit to the 325 K data, olive green curve. The two Gaussian components are the dashed purple and dark cyan curves. At all temperatures, the large, broad peak completely subsumes the smaller one. Also, at all temperatures, the smaller peak that arises from the best fit has nearly identical spectral parameters as those observed in the non-H-bonding liquid, BZP. This indicates that there are two distinct populations in the liquid: an H-bonding and a non-bonding population. As there are also unambiguously H-bonding and non-bonding hydroxyls in the neat BPM liquid at all temperatures,[33] this fit is justified. The proposition of two distinct subensembles is confirmed by the pump-probe data presented below.

C. Polarization selective pump-probe spectroscopy

The optical setup and experimental methods for ultrafast IR experiments have been thoroughly described in previous publications.[16,44] Briefly, a Ti:sapphire oscillator and regenerative amplifier produced ultrafast pulses at 800 nm and a 1 kHz repetition rate. The 800 nm pulses were used to pump an optical parametric amplifier to produce pulses in the mid-IR (4.6 μm, 120 fs duration, and 6 μJ/pulse). The pulses were then controlled temporally through the use of precision mechanical delay stages over a range of nearly 2 ns with sub-femtosecond accuracy.

For pump-probe experiments, each mid-IR pulse is divided into a strong pump pulse and a weak probe pulse. The pump pulse polarization was rotated 45° relative to the probe pulse polarization, after which the pump and probe are crossed spatially in the sample. The probe is then frequency resolved with a spectrograph and collected on a 32 pixel mercury-cadmium-telluride array detector. By resolving the probe pulse at polarizations parallel and perpendicular to the pump pulse (±45°), the isotropic (population) and anisotropic (orientational) relaxation of the PhSeCN probe molecule can be determined as follows:[45]

$$P(t) = \frac{1}{3}\left(I_{\parallel} + 2I_{\perp}\right),$$
$$r(t) = 0.4C_2(t) = \frac{I_{\parallel} - I_{\perp}}{I_{\parallel} + 2I_{\perp}}, \quad (1)$$

where $I_{\parallel}$ and $I_{\perp}$ are the signal intensity for the parallel and perpendicular polarizations, respectively; $P(t)$ is the isotropic population relaxation; $r(t)$ is the anisotropic orientational relaxation; and $C_2(t)$ is the second Legendre polynomial orientational correlation

Published under license by AIP Publishing

function. The population decay is generally exponential in time barring more complex phenomena. The anisotropic decay, in contrast, is typically not a single exponential.

As has been seen previously for PhSeCN, there was no strong temperature dependence in the population relaxation of the CN stretch for PhSeCN in 2BPM.[37,38] In contrast to what is usually seen for nitrile modes, the population relaxation has a strong frequency dependence, where fits to a single exponential decay yield vibrational lifetimes of about 380 ps at the maximum to about 200 ps on the blue wing. Employing instead a global fit of the frequency dependent population decays with a biexponential function having two shared time constants (performed from 100 ps to 1800 ps to avoid various possible early time phenomena) yields a more complete picture. The relative amplitudes of the two time constants trace out a narrow spectrum with a long lifetime (~425 ps) and a wider spectrum with a shorter lifetime (~225 ps). Figure 2 displays the amplitudes of the two components of the lifetime fits as a function of wavelength. The positive-going, higher frequency portion arises from the 0-1 transitions (ground state to 1st vibrational excited state). The negative bands are from the 1-2 transitions and are shifted to lower frequency because of the vibrational anharmonicity. The center frequencies and FWHM of these bands match those seen from the decomposition of the linear spectrum into two components (Fig. 1, dashed purple and dark cyan curves). Furthermore, the narrow band's vibrational lifetime closely matches that of PhSeCN in non-H-bonding liquids, and H-bonding typically results in a shorter vibrational lifetime. These observations confirm the separation of the IR spectrum into two separate but heavily overlapped peaks, corresponding to hydrogen-bonding and non-bonding probe populations.

The pump-probe anisotropy, which reports on the orientational relaxation of the vibrational probe, displayed a strong temperature dependence (Fig. 3). This is similar to previous observations in other glass forming liquids.[37] At all temperatures, there is some deviation from perfect correlation [$r(0)$ = 0.4, Eq. (1)] at zero waiting time, which corresponds to the existence of subpicosecond "inertial" motions that occur on time scales faster than the IR pulse duration. The relaxation is also multi-component at all temperatures, with a fast motion of ~10 ps that decreases in amplitude as the temperature is lowered, and a slow motion that makes up the rest of the decay that slows dramatically with decreasing temperature.

In contrast to the vibrational lifetime, the anisotropy was found to be almost completely frequency independent. This is surprising, given that our decomposition of the IR spectra into hydrogen-bonding and non-bonding components would seem to imply that the two populations would have different dynamics as well. As will be shown in Sec. III C this frequency independence can be explained by exchange between these two populations.

In comparison to the anisotropies measured for PhSeCN in the non-H-bonding glass forming liquid BZP, the anisotropies are nearly quantitatively identical when rescaled to their respective glass transition temperatures (T_g = 236 K for PhSeCN/2BPM and 212 K for PhSeCN/BZP[38]), as shown in Fig. 3. As both BZP and 2BPM have similar "fragilities,"[31,32] meaning that they have approximately the same α-relaxation time scales and viscosities when they have the same temperature differences from their glass transitions,[22] this suggests that the anisotropy is almost entirely set by the viscosity of the liquid. This rescaling is effective for the amplitudes and time scales of the fast orientational motions as well as for the slow orientational diffusion that might be expected from the Stokes-Einstein-Debye relation.

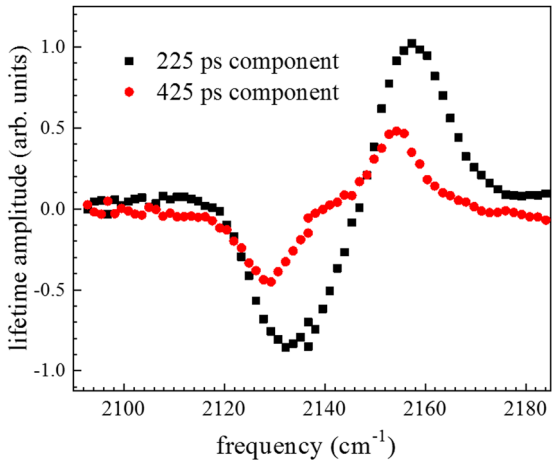

FIG. 2. Frequency dependent amplitudes of a biexponential fit to the isotropic pump-probe decay of PhSeCN in 2BPM at 300 K. The positive going higher frequency portion arises from the 0-1 transitions (ground state to 1st vibrational excited state). The negative bands are from the 1-2 transition and are shifted to lower frequency because of the vibrational anharmonicity. The amplitudes of the two component decays trace out two spectra with differing vibrational lifetimes. The spectra match closely the spectra obtained from the decomposition of the FT-IR spectrum into two peaks (Fig. 1). The smaller, narrower peak (red) had a vibrational lifetime very similar to that of PhSeCN in non-H-bonding liquids. The shorter lifetime and broader spectra of the other peak (black) are consistent with the observations of H-bonded nitriles.

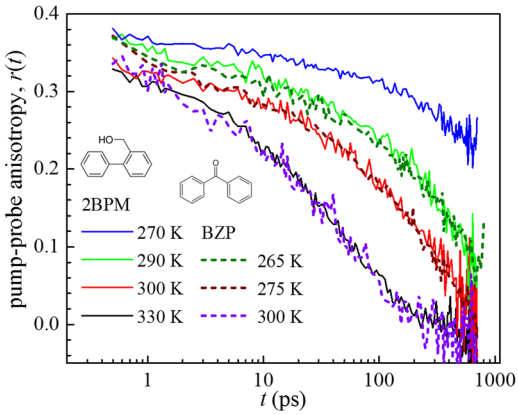

FIG. 3. Temperature dependent anisotropic pump-probe decays of PhSeCN in 2BPM. Unlike the isotropic decay, the anisotropic decay was found to be strongly temperature dependent and largely frequency independent. When rescaled to their respective T_g's, the anisotropic decay of PhSeCN in 2BPM was found to be nearly quantitatively identical to that of PhSeCN in BZP (structure depicted), a non-H-bonding glass forming liquid.

Published under license by AIP Publishing

D. 2D IR vibrational echo spectroscopy

The 2D IR experiment uses the same experimental setup as the pump-probe experiment. For polarization-selective 2D IR experiments, each mid-IR pulse is divided into three pulses of approximately equal intensity, as well as a fourth, much weaker pulse to serve as a local oscillator (LO). The three pulses are crossed spatially in the sample in BoxCARS geometry so that the echo signal propagates in a different direction from the incident pulses. No additional polarization optics are then necessary to obtain the ⟨XXXX⟩ polarization. To obtain the ⟨XXYY⟩ polarization, half wave plates and polarizers are used to set the first two beams at 90° relative to the native horizontal polarization of the IR laser.

To generate a 2D spectra, the time delay between first and second incident pulses (τ) is scanned while the delay between the second and third pulses (waiting time, T_w) is held constant. The first two pulses effectively label the probe molecules with their initial frequencies. During the waiting time, T_w, structural fluctuations of the liquid, which change local and mesoscopic intermolecular interactions, will cause the frequencies of the probe molecules to evolve from their initial values. After letting the system evolve for the duration of T_w, the third pulse stimulates the emission of the echo signal. The echo signal is then combined with and heterodyned by the LO pulse to provide phase information. The combined echo/LO is frequency resolved using the spectrograph and array detector as in the pump-probe experiment. Scanning τ produces a time-domain interferogram on each pixel of the array detector. The array detector data provide the vertical axis of the 2D spectra (ω_3), while a numerical Fourier transform of the interferogram provides the horizontal axis (ω_1), corresponding to the final and initial frequencies of the oscillators at a given waiting time, T_w, respectively. Data acquisition times are greatly reduced by working in a rotating frame,[46] which enables sampling fewer time points to generate a full interferogram.

The 2D spectra then encode dynamical information in its line shape, which is dependent on the FFCF. At waiting times that are short compared to the structural fluctuations of the sample, the initial and final frequencies will be highly correlated and give an elongated line shape. If the waiting time is long compared to the structural fluctuations of the sample, the initial and final frequencies will decorrelate and result in a rounder line shape. This evolution can be quantified with the Center Line Slope (CLS) method,[47,48] which slices the spectra parallel to the ω_3 axis and finds the maxima of each slice. The slope of these maxima with respect to ω_1 then yields the normalized FFCF for the given waiting time. The complete FFCF is typically modeled as a sum of exponentials with a Kubo line shape function[17,49]

$$C(t) = \langle \delta\omega(t)\delta\omega(0)\rangle = \frac{\delta(t)}{T_2} + \sum_i \Delta_i^2 \exp(-t/t_i), \tag{2}$$

where $\delta\omega$ is the instantaneous frequency fluctuation at time t, $\delta(t)$ is the Dirac delta function, T_2 is the total homogeneous dephasing time (inversely related to the homogeneous linewidth), Δ_i is the frequency fluctuation amplitude of the ith component of the inhomogeneous line shape, and t_i is the corresponding correlation time of that component. The complete FFCF can be obtained through simultaneous fitting of the CLS and the FT-IR line shape.[39,40]

As discussed briefly above, the observed FFCF can change based on the polarization of the pulses, RISD.[11,12] For a vibrational probe with a permanent dipole moment undergoing orientational diffusion in a relatively slowly evolving electric field, the RISD contribution to spectral diffusion can be obtained analytically to yield the following expressions:[12]

$$\begin{aligned}\langle \delta\omega(t)\delta\omega(0)\rangle_{\text{para}} &= \frac{3}{25}\left[\frac{11C_1(t)+4C_3(t)}{1+0.8C_2(t)}\right]\times \text{SSD}(t),\\ \langle \delta\omega(t)\delta\omega(0)\rangle_{\text{perp}} &= \frac{3}{25}\left[\frac{7C_1(t)-2C_3(t)}{1-0.4C_2(t)}\right]\times \text{SSD}(t),\end{aligned} \tag{3}$$

where C_l is the lth order Legendre polynomial time correlation function and SSD(t) is the structural spectral diffusion caused by fluctuations in the environment. In the case of orientational diffusion, $C_l = \exp(-l(l+1)Dt)$. All of the C_l's can be determined from the C_2 correlation function measured with the pump-probe anisotropy experiments [Eq. (1)], in principle allowing for the separation of the structural spectral diffusion (SSD) dynamics from the RISD effect.[12]

Polarization selective 2D IR spectra were taken for PhSeCN in 2BPM over a range of temperatures, from 355 K to 270 K. Several CLS decays are shown in Fig. 4, with solid symbols corresponding to the parallel ⟨XXXX⟩ polarization configuration and open symbols to the perpendicular ⟨XXYY⟩ configuration. From the CLS decays, it can be seen that 2BPM exhibits the same basic behavior that has previously been seen in the spectral diffusion of PhSeCN in other glass forming liquids.[37,38] The CLS decays first have a fast, picosecond time scale decay which decreases in amplitude rapidly with

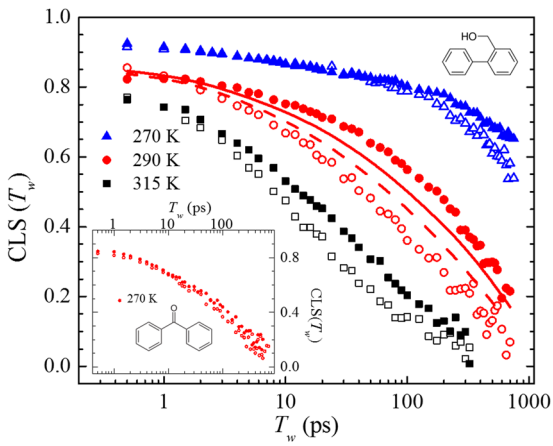

FIG. 4. Temperature and polarization dependent CLS decays of PhSeCN in 2BPM. The solid symbols correspond to the parallel ⟨XXXX⟩ polarization configuration, while the open symbols correspond to the perpendicular ⟨XXYY⟩ polarization configuration. The significant temperature dependence is similar to what was seen in other glass forming liquids with the PhSeCN probe. Significant polarization dependence of the dynamics is observed at all temperatures, most prominently at moderate supercooling (~290 K). Red solid and dashed curves are fits to the data at 290 K using the standard RISD theory, demonstrating that the observed polarization dependence is far in excess of the RISD predictions. Inset: CLS decays of PhSeCN in the non-H-bonding glass forming liquid BZP (structure depicted) at moderate supercooling show almost no polarization dependence. The very large polarization effect seen in 2BPM can then be attributed to H-bonding.

Published under license by AIP Publishing

decreasing temperature. There is then a slower, final decay which dramatically slows as the temperature is lowered. This behavior in the CLS decays is qualitatively similar to the temperature-dependent behavior of the pump-probe anisotropy data shown in Fig. 3.

However, 2BPM exhibits a remarkable polarization dependence, particularly for moderate supercooling, in sharp contrast to the behavior of non-H-bonding liquids such as BZP. Even above the melting point (321 K), there is a noticeable difference between the two measurements in 2BPM (see the supplementary material). In Fig. 4, the 290 K parallel data (red filled circles) are very different from the perpendicular data (red open circles). These data should be compared to the data in the inset for BZP at 270 K, which is approximately the same temperature difference from T_g as the 290 K 2BPM data. The BZP data in the inset show little difference between parallel and perpendicular configurations.

The PhSeCN probe exhibits the same orientational relaxation in 2BPM and BZP at the same rescaled temperature (Fig. 3), so the 2D IR polarization dependence in 2BPM is not explained through different reorientational motions. The observed differences between the polarizations are substantially greater than predicted by the RISD vibrational stark effect model used to derive Eq. (3). For example, at 290 K, global fits (solid and dashed red curves, Fig. 4) employing Eq. (3) with the measured orientational relaxation times fail to describe the magnitude of the polarization difference between the data (red symbols).

A possible explanation for this very large RISD arises from the observation that there are two distinct populations of PhSeCN in 2BPM, H-bonding and non-bonding. The existence of two populations is supported by the frequency dependence of the vibrational lifetime (Fig. 2) and line shape fitting of the linear FT-IR spectra (Fig. 1), as well as from observation of non-H-bonding hydroxyls in the FT-IR spectra at all temperatures. As discussed below, the observed differences in the two polarizations arise from chemical exchange between the two populations with a relatively large angular change, as illustrated in Fig. 5.

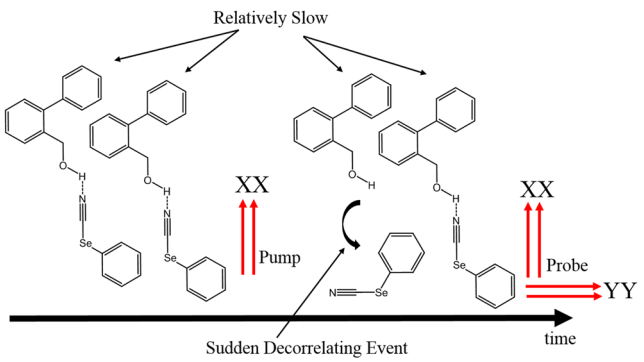

FIG. 5. Illustration of an example XISD process for PhSeCN in 2BPM. At t = 0, both probe molecules are H-bonded to 2BPM molecules and are labeled by the first two pulses in the 2D IR experiment. During the waiting time T_w, one of the PhSeCN molecules reorients, breaking the H-bond and placing itself in the non-bonded population. This decorrelates its frequency. After T_w, the final pulse in the 2D IR experiment reads the final frequency. If the final frequency is read off in the same polarization, it will be biased to probe the non-exchanged PhSeCN, which will be highly correlated. If it is read off in the orthogonal polarization, it will be biased to the decorrelated exchange population.

III. MODELING EXCHANGE-INDUCED SPECTRAL DIFFUSION

A. Chemical exchange and jump exchange in 2D IR spectroscopy

Chemical exchange is exhibited in a 2D IR spectrum when the probe can exchange from one type of species to a different species with the two species having distinct vibrational absorption spectra, e.g., going from H-bonded (HB) to non H-bonded (NB) and vice versa. Two spectra are associated with these species. Chemical exchange is different from spectral diffusion in which the probe experiences continuous, time dependent intermolecular interactions because of changes in the structure of the medium while remaining the same type of species. If chemical exchange occurs on the time scale of the 2D IR experiment, it will be manifested in the 2D spectra through the growth of off-diagonal peaks (cross-peaks).[7,8,16,44,50–52] As a cross-peak has the initial frequency of one chemical species and the final frequency of the other species, it is typically only considered when there are two at least partially separated peaks in the linear spectra. The time dependence of the growth of the cross-peaks provides information on the kinetics of the exchange.

The exchange event generally involves decorrelation of the frequency because the frequency of the probe vibration in one chemical environment is uncorrelated with the frequency in another distinct type of environment.[50] Furthermore, if probes exchange their chemical environments an even number of times, i.e., they start and end as the same species, this subensemble will contribute a completely decorrelated frequency component (round component) to the diagonal line shape.[50]

It has also been demonstrated that chemical exchange can have a significant angular dependence, resulting in differing intensities of cross peaks in parallel and perpendicular pulse geometries.[7,8] This phenomenon has been most notably observed in water-ion solutions, where the proposed mechanism is a concerted angular "jump" between a water-water H-bond and a water-ion H-bond. The relative intensities of the cross and diagonal peaks in the two polarization schemes provided information on the jump angle in the system.[7,8] While the model was developed for a specific, concerted hydrogen-bond rearrangement mechanism, it is reasonable to apply the same ideas to any chemical exchange where an orientational change is expected. Despite the difference in the chemical systems, we will refer to the angle associated with the exchange process as the "jump angle" for consistency.

While chemical exchange is typically only explicitly studied when there is a significant spectral shift between chemical species, chemical exchange can still occur between species with heavily overlapped spectra. In this situation, the two diagonal peaks and the two cross-peaks overlap forming one spectral feature. However, if there is an angular dependence to the exchange that results in a strong polarization dependence of the intensity of the cross peaks, then the exchange will create a polarization dependence for the overall 2D line shape. The CLS measurement on this line shape will then depend on the relative intensities of these exchange peaks as well as the standard spectral diffusion exhibited by the non-exchanging populations. Simulating the experimental line shapes requires the calculation of the relative populations seen in each polarization as well as calculation of the diagonal and cross peak line shapes.

Published under license by AIP Publishing

B. Calculating 2D spectra with the jump exchange kinetic model

To explain the large polarization dependence of the CLS measurement of PhSeCN in 2BPM (see Fig. 4), the chemical system will be modeled as a large-angle jump exchange of PhSeCN molecules between H-bonded and non-bonded states, with the spectra of the H-bonded and non-bonded species heavily overlapped, as described in Sec. II. The observed 2D spectra are then the linear combinations of six spectra: two diagonal non-exchanged peaks that exhibit non-exchange spectral diffusion, and four off-diagonal exchange peaks, which depend only on the initial and final species of a given probe. Example spectra of each type are given in Fig. 6. The top row shows diagonal bands as there is no exchange. The second and third rows show off-diagonal bands only. The amplitudes of these peaks are time dependent in accord with the jump exchange kinetic equations, but spectral diffusion makes the line shapes of the non-exchanging peaks time dependent as well.

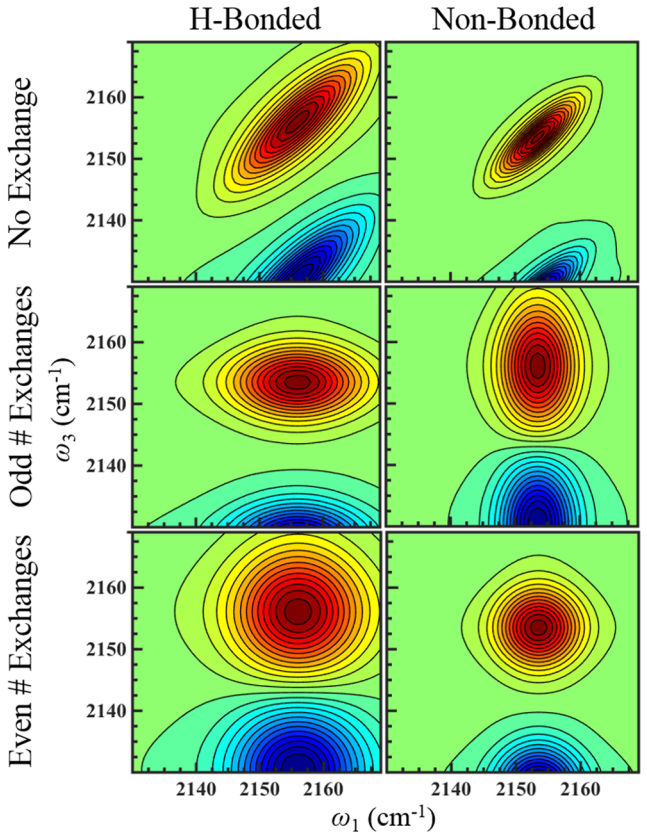

FIG. 6. The component peaks used in modeling exchange-induced spectral diffusion at 300 K, based on the decomposition seen in the FT-IR spectra (Fig. 1) and isotropic pump-probe decays (Fig. 2). The spectra in the left column correspond to PhSeCN molecules that are H-bonded (HB) at $T_w = 0$, while the right column correspond to those that are not H-bonded (NB). The top row shows diagonal bands as there is no exchange. The middle row bands are the off-diagonal peaks that arise for probes that have undergone a single (or odd-number of) exchange(s), and the bottom row shows diagonal bands that arise from an even number of exchanges. The experimental spectra are then a linear combination of these six component spectra.

Calculating the polarization-dependent 2D IR spectra, CLS, and pump-probe anisotropy decays with this method requires the input of spectral properties, the rates and jump angles in the kinetic model, and the non-exchange structural spectral diffusion (SSD) parameters of each peak. The time-independent spectral properties can be reasonably well determined from the pump-probe data and the two-peak fit of the linear FT-IR spectra discussed previously. From these two measurements, it is possible to get reasonable values for the relative population sizes (N_{HB}/N_{NB}), the relative transition dipole strengths (μ_{HB}/μ_{NB}), center frequencies ($\langle\omega\rangle$), anharmonic shifts ($\langle\omega_{12}\rangle$), and total widths ($\Delta$) of the two component peaks. The calculations of these properties are detailed in the supplementary material, and the results are summarized in Table I.

The kinetic equations that govern jump exchange have been developed in detail by Ji and Gaffney,[7] and the relevant results as well as minor modifications for this work are described in the supplementary material. Qualitatively, the kinetic equations are differential equations that describe the time evolution of the magnitude of the two species' populations. In this case, the species are hydrogen-bonded and non-bonded PhSeCN. The equations are subdivided into an isotropic part, which includes the lifetime decay of each species and the chemical exchange rate, and an anisotropic part that adds the orientational motion of the two species. Of particular importance, the anisotropic part also includes an angular dependence for the chemical exchange, which is the aforementioned "jump" angle Θ. The jump angle and the three rates of the kinetic model can fully describe the magnitude of each population that appears in a given polarization, given the information on the relative equilibrium population sizes and transition dipole strengths.

The non-exchanging FFCFs describe structural spectral diffusion (SSD), i.e., the spectral diffusion exhibited by the probe that is not induced by the orientational motion or chemical exchange of the probe.[11] The SSD is caused by the structural dynamics of the surrounding 2BPM supercooled liquid. The two species, HB and NB, will have different SSD, particularly as the H-bond interaction will contribute significantly to spectral diffusion. Any dynamics that causes fluctuations in the H-bond length or orientation (while not breaking the bond) will cause SSD,[19,41] but will not appear in the NB population's SSD, causing the HB SSD to decay faster.

The majority of the time-dependent parameters in the kinetic model and SSDs were determined through nonlinear fitting to the polarization dependent CLS decays and the pump-probe anisotropy

TABLE I. Component peak time-independent parameters. $\langle\omega\rangle$, $\langle\Delta\omega_{12}\rangle$, and Δ are the center frequencies, vibrational anharmonicities, and FWHM's of the given spectrum, respectively. N and μ are the equilibrium population size and transition dipole of the given species, respectively.

	$\langle\omega\rangle$ (cm^{-1})	$\langle\Delta\omega_{12}\rangle$ (cm^{-1})	Δ (cm^{-1})	N/N_{NB}	μ^2/μ^2_{NB}
HB	2157–58	25.5	5.2–5.6	0.9	3.8
NB	2153.5	25.5	3.8	1	1

Published under license by AIP Publishing

decays for a given temperature. Most of the kinetic model parameters were found to be well determined from the pump-probe anisotropy. Due to the heavy overlap of the non-exchange peaks and the growing overlapping cross peaks, the SSD terms tended to have the largest fitting uncertainty. Additional details about the fitting procedure can be found in the supplementary material. When reasonable parameters were obtained from the fits, the model was found to be able to be used to calculate the experimental polarization dependence of the 2D line shapes (Fig. 7). As shown in Fig. 7, the calculation was also able to describe the 2D anisotropic spectrum (⟨XXXX⟩ − ⟨XXYY⟩), which enhances the anisotropic elements while suppressing the isotropic elements.

C. Modeling non-exponential orientational relaxation

The last experimental feature that has to be accounted for is the non-exponential nature of the orientational relaxation as seen in the pump-probe anisotropy data. There are two broad categories of behavior that can result in a non-exponential relaxation: a homogeneous model, where every probe molecule in a population exhibits the same multi-step orientational relaxation, and a heterogeneous model, where different subensembles of probes exhibit different simple relaxations that result in a non-exponential relaxation when averaged in the experimental observable. In general, it is impossible for two-time correlation functions, such as the orientational relaxation measured by the IR pump-probe or the FFCF measured by 2D IR, to distinguish between the two possibilities.[53] We will demonstrate that in certain circumstances XISD can distinguish between these two pictures.

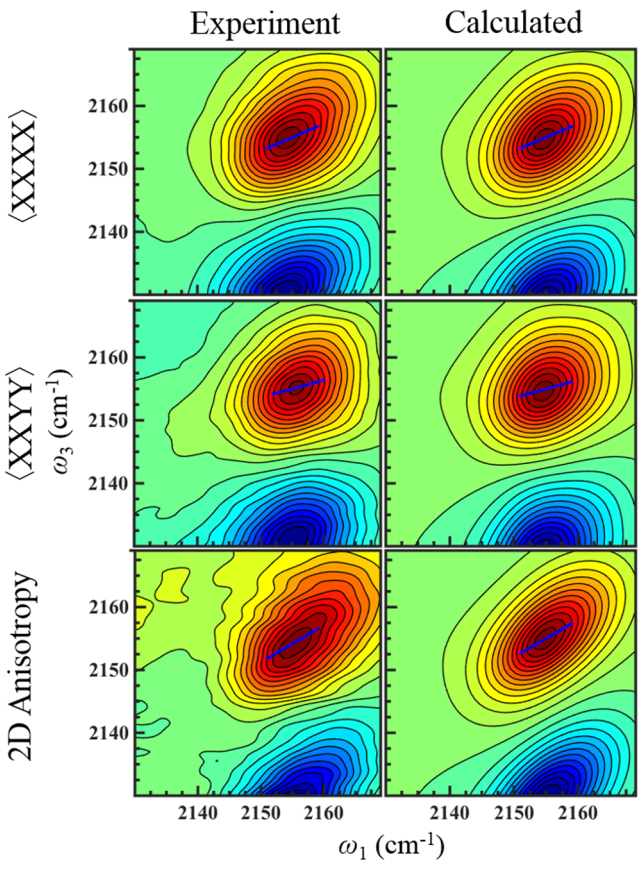

FIG. 7. Comparison of experimental 2D IR spectra (left) and calculated spectra (right) from the XISD model of PhSeCN in 2BPM for 300 K at T_w = 100 ps. Top: ⟨XXXX⟩ spectra; middle: ⟨XXYY⟩ spectra; and bottom: 2D anisotropic spectra. Blue lines correspond to the Center Line Slope (CLS) of the 2D spectra, a measure of correlation.

1. Homogeneous "wobbling-in-a-cone" dynamics

A method for addressing the non-exponential behavior uses the "wobbling-in-a-cone" model, in which the probe undergoes a restricted angle diffusive process before constraint release enables complete orientational relaxation.[54,55] The model can be used for any number of increasingly less restricting cones.[54,55] As discussed in Sec. II C, one way the anisotropy of PhSeCN in BPM can be described has a sub-picosecond "inertial" drop that accounts for deviations from perfect correlation at very short time,[56] an additional diffusive cone, and final orientational randomization. The mathematics of using the wobbling description in the kinetic model is described in the supplementary material. The wobbling parameters can be characterized almost completely from the pump-probe anisotropy data.

The results of a nonlinear fit of the wobbling XISD model to the experimental data at 300 K show that XISD is capable of reproducing the large difference between the two polarization-dependent CLS decays but only at long (>200 ps) T_w's [Fig. 8(a), blue curves]. A significant jump angle is necessary to give the observed dynamics, 30° or more. The time scale of orientational randomization caused by a given exchange rate and jump angle Θ is given by

$$\tau_{D,ex} = \tau_{ex}\left[1 - \langle P_2(\cos\Theta)\rangle\right]^{-1}, \quad (4)$$

where τ_{ex} is the isotropic exchange time. The best fits with the wobbling model yields $\tau_{D,ex}$ that is essentially identical to the time scale of orientational relaxation measured by the pump-probe anisotropy. Because exchange with a large jump angle can reproduce the long time data, the non-exchange, complete orientational diffusion rates, also contribute to the pump-probe anisotropy decay, must be very small. The calculated $\tau_{D,ex}$ and very small complete diffusion rates suggest that the exchange between the populations is the principle manner of reorientation. The primarily exchange-based reorientation is further supported by the frequency independence of the pump-probe anisotropy, as significant and different diffusion rates for the H-bonded and non-bonded species would cause some parts of the spectrum to orientationally relax faster than others.

Although the wobbling model with exchange jump reorientation can describe the data at long time [Fig. 8(a) blue curves], it misses noticeably at intermediate times (10 ps–100 ps). It also dramatically misses the CLS of the 2D anisotropic spectra (⟨XXXX⟩ − ⟨XXYY⟩) from ~10 ps on [Fig. 8(c), blue curve]. On the intermediate time scale, the wobbling model cannot sufficiently move population between the subensembles that contribute predominately to the parallel and perpendicular CLS observables. To replicate the differences between the various CLS decays over the full time range, it is necessary to examine models that permit large angle reorientation through chemical exchange at intermediate times.

Published under license by AIP Publishing

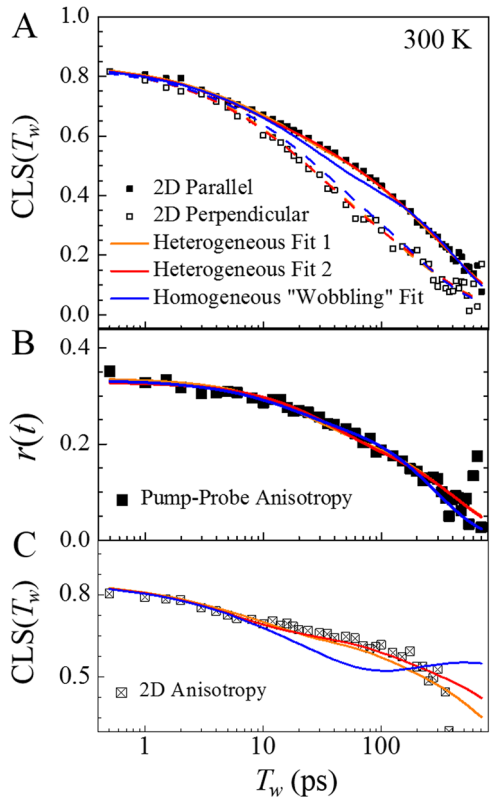

FIG. 8. (a) Fits of XISD models to experimental 2D IR data of PhSeCN in 2BPM at 300 K. Solid black squares correspond to the experimental ⟨XXXX⟩ polarization data, and the open black squares correspond to ⟨XXYY⟩ polarization data. Solid curves are fits to the ⟨XXXX⟩ data, and dashed curves are fits to the ⟨XXYY⟩ data. It can be seen that the heterogeneous exchange models (red and orange curves) fit the experimental data at all times, while the "wobbling" homogeneous exchange model (blue curves) misses at intermediate times. (b) Experimental pump-probe anisotropy (orientational relaxation) fit with all models. All models describe the decay well. (c) CLS decay of the 2D anisotropic spectra. The heterogeneous models fit very well, while the "wobbling" model misses after short time.

2. Heterogeneous orientational dynamics

Over the past three decades, the presence of heterogeneous dynamics in supercooled liquids and glasses has become well established.[53,57–59] This heterogeneity manifests as differing molecular relaxation rates in different spatial regions of a liquid at a given time. Due in part to experimental limitations, the vast majority of experimental evidence for dynamical heterogeneity appears near the glass transition and in the slowest dynamics, i.e., the α-relaxation, on time scales of nanoseconds and mainly much longer. However, there is some experimental evidence for heterogeneity in density fluctuations in a wide class of glass forming materials on picosecond time scales.[25] There is also some evidence from simulations of heterogeneous reorientation on fast time scales, generally as part of a large distribution of reorientation times.[60–64]

A model that can be employed to describe heterogeneous dynamics assumes that every subensemble of molecule relaxes exponentially.[53] The observed non-exponential decay occurs from averaging the subensembles that have different exponential relaxation rates. As the experimental pump-probe anisotropy decays fit well at all temperatures to a biexponential function, two populations are sufficient for our model: one with a fast exchange/reorientation time and the other with a slow exchange/reorientation time.

These dynamical populations are distinct from the HB and NB populations, which are spectroscopically separable as different species, and we assume that the same proportion of the HB and NB species are in the fast and slow subensembles. This assumption, in addition to simplifying the calculations, is justified by the frequency independence of the pump-probe anisotropy decays. It is also necessary to maintain the inertial component to account for the initial subpicosecond orientational relaxation discussed in Sec. II. The inertial component gives rise to the initial value of <0.4 observed in the anisotropy decays.

A major consideration in heterogeneous models is the persistence time of the different subensembles that exhibit distinct dynamics. As a liquid above the glass transition is physically homogeneous and ergodic, the fast and slow subensembles (and the corresponding spatial domains in the liquid exhibiting these dynamics) must interconvert on some time scale.[53] The two extremes of this time scale were investigated. One has the dynamical subensembles not interconverting on the relatively short 2D IR time scale (<1 ns), and the other has the subensembles interconverting on the time scale of the slow reorientational dynamics (Fig. 9, top and bottom, respectively).

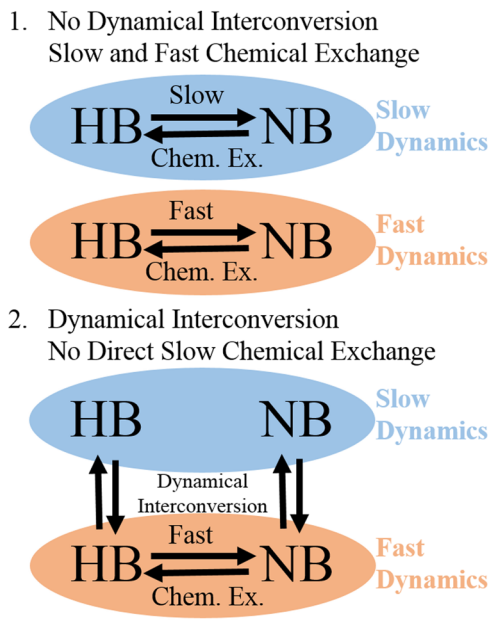

FIG. 9. Illustration of the two different heterogeneous exchange models described in Sec. III. The first has no interconversion between the "slow" and "fast" dynamical subensembles on the experimental time scale but has slow and fast chemical exchange rates for both slow and fast subensembles. The second has dynamical interconversion between slow and fast dynamical subensembles on the experimental time scale, but no chemical exchange between the slow dynamics species on experimental time scales. The two models were found to be essentially indistinguishable when used to fit the data, but arguments from the thermodynamics of exchange can be used in favor of the second model.

Published under license by AIP Publishing

Implementing either of the models depicted in Fig. 9 requires only modifications to the kinetic model. The details are given in the supplementary material. The implementations were designed to preserve the same number of parameters as the homogeneous wobbling model to avoid improving the fits from over-parameterization.

Both heterogeneous models fit the data very well on all time scales and provide better fits than the wobbling model. The results of the fits are shown in Fig. 8 as red and orange curves. In Figs. 8(a) and 8(b), the two curves are indistinguishable and appear as one curve. To fit the data, it was necessary to have larger magnitude angular motions at early time that are associated with decorrelating the line shape preferentially in the ⟨XXYY⟩ polarization, which both heterogeneous models provide. The agreement between the data and the fits shown in Fig. 8 holds over the entire range of temperatures studied (see the supplementary material).

As shown in Fig. 8, the two heterogeneous models are nearly quantitatively identical, with almost the same parameters providing essentially the same fit lines. The parameters are also nearly the same for the two models at all temperatures studied. Thus, the experimental data cannot tell the difference between two persistent dynamical populations for the duration of the experiment, and interconversion between the fast and slow dynamical populations on the experimental time scale. Slow interconversion in model 2 replaces slow chemical exchange in model 1 to produce apparent slow chemical exchange. Therefore, the observation of what appears to be slow chemical exchange dynamics can arise from either model. The observed slow chemical exchange discussed below could arise in either manner depicted by models 1 and 2. Because of their similarity, discussions in Sec. IV treat these models interchangeably unless otherwise noted.

IV. XISD BEST FITS AND TEMPERATURE DEPENDENCE OF 2BPM DYNAMICS

The two heterogeneous kinetic models were employed to describe the pump-probe anisotropy and polarization-dependent CLS decays at a series of temperatures, 355 K–270 K, from well above the melting temperature T_m (321 K) through deep supercooling. Parameters relating to the vibrational lifetime, vibrational dephasing time (T_2), and time-independent spectral properties were set by separate experiments (see the supplementary material). The non-exchanging FFCFs were able to be described as a biexponential for each species. Five kinetic model parameters (2 exchange rates, τ_{ex}; jump angle, Θ; inertial cone parameter, T^2; and fraction of probes that are dynamically slow, f) and six FFCF parameters (2 time constants, τ, and their relative amplitudes, Δ, for each species' FFCF) were allowed to vary.

A. Heterogeneity of exchange

The fraction f of the population that exhibited the slow exchange dynamics, and thus, the slow orientational motion, was found to be highly temperature dependent (see Table II). f varied from about 25% of the population at 355 K to 85% of the population at 270 K, presumably with f continuing to increase as the glass transition is approached. Assuming a Boltzmann distribution (from $f/[1-f]$), the activation energy to go from the slow to fast states is 23.3 ± 1.5 kJ/mol. Extrapolated to the glass transition (236 K), this activation energy implies that less than 5% of the probes should exhibit picosecond timescale exchange dynamics at T_g, with the majority of molecules locked into their hydrogen-bonded or non-bonded states. The large activation energy combined with the large population in the fast subensemble also implies that there are vastly more structural configurations available to the dynamically fast probes, but the system can become thermally trapped in the set of slow states.

One possible candidate for a maximum in heterogeneity is f = 50%, which occurs at ~325 K. This temperature is near the melting temperature of the 2BPM. 325 K also corresponds to ~1.4 T_g, the same scaled temperature at which dynamic heterogeneity in slow spectral diffusion appeared in non-H-bonding liquids.[38] The temperature ~1.4 T_g has previously been associated with the onset of heterogeneous dynamics in simulations of glassy behavior.[65–67]

In addition to the percentages of populations exhibiting slow and fast dynamics, there is a sharply increasing separation in time scale between them as the temperature is decreased. From 355 K to 270 K, the slow exchange time scale grew from 40 ps to 5000 ps ($\tau_{ex,slow}$ in Table II), while the fast exchange time scale only varied between 7 and 20 ps ($\tau_{ex,fast}$ in Table II). The similarity in the fast

TABLE II. Heterogeneous exchange kinetic model fit parameters. $\tau_{ex,slow}$ and $\tau_{ex,fast}$ are the two exchange time scales of an NB species to an HB species. The reverse rates can be readily determined from the equilibrium condition. Θ is the jump angle, f is the percent of population in the slow subensemble, and T^2 is the inertial wobbling order parameter.

T (K)	Θ (deg)	$\log[\tau_{ex,slow}/\text{ps}]$	f	$\log[\tau_{ex,fast}/\text{ps}]$	T^2
355	47 ± 7	1.6 ± 0.2	0.26 ± 0.06	1.1 ± 0.1	0.79 ± 0.03
345	47 ± 6	1.7 ± 0.1	0.38 ± 0.04	0.9 ± 0.2	0.87 ± 0.03
335	44 ± 6	1.9 ± 0.1	0.38 ± 0.05	1.0 ± 0.1	0.88 ± 0.03
325	44 ± 4	1.8 ± 0.1	0.51 ± 0.08	0.8 ± 0.2	0.79 ± 0.03
315	44 ± 3	2.1 ± 0.1	0.62 ± 0.04	0.9 ± 0.2	0.87 ± 0.03
300	45 ± 5	2.6 ± 0.1	0.60 ± 0.04	1.3 ± 0.2	0.83 ± 0.03
290	50 ± 7	2.7 ± 0.1	0.70 ± 0.03	1.1 ± 0.3	0.94 ± 0.03
280	55 ± 9	3.3 ± 0.1	0.74 ± 0.02	1.4 ± 0.3	0.97 ± 0.03
270	51 ± 10	3.7 ± 0.5	0.86 ± 0.03	1.0 ± 0.4	0.92 ± 0.03

Published under license by AIP Publishing

and slow exchange rates at high temperatures made it relatively difficult to distinguish the heterogeneous nature of the dynamics from purely homogeneous dynamics.

It is the substantial separation of time scales at moderate supercooling, along with significant population in both dynamical subensembles, which enabled the identification of heterogeneity, as displayed in Fig. 8. As the time scales of the fast and slow dynamics become more similar (i.e., at high temperatures) or the fast subensemble becomes sparsely populated (i.e., at low temperatures), the difference in the predictions of the heterogeneous models and the homogeneous model becomes smaller. These extremes are illustrated in the supplementary material.

Experimental evidence for significant picosecond time scale dynamical heterogeneity in glass formers is significant, as most attention has been paid to the alpha relaxation on long time scales.[53] The picosecond time scale dynamical heterogeneity reported here is in the orientational motion of the probe. Previous evidence of picosecond-scale heterogeneity is limited to quasi-elastic neutron scattering and simulation results, which are primarily concerned with the time and length scales of density fluctuations,[25] with only a relatively small number of simulations describing orientational heterogeneity.[60–64]

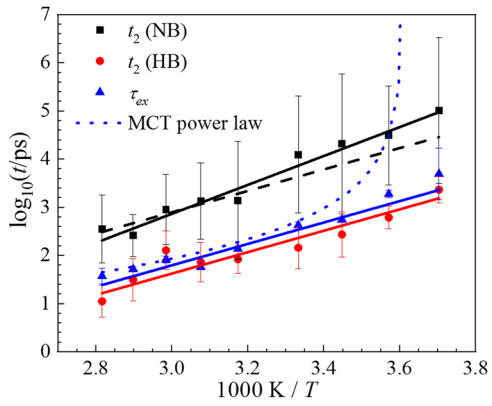

FIG. 10. Arrhenius plot of the slow dynamics in the PhSeCN in the 2BPM system. Slow exchange time—blue triangles. Slow term of the structural spectral diffusion, HB species—red circles. Slow term of the structural spectral diffusion, NB species—black squares. The solid lines are the best fits to the data sets. The black dashed line has the same slope as the red and blue lines. There is no indication of power-law like temperature dependence, as was measured in 2BPM using OKE spectroscopy (blue dashed curve) or measured in non-H-bonding glass forming liquids using 2D IR.

B. The jump angle

The "jump" angle Θ, or more specifically, the average large angle shift associated with an exchange, was neither strongly temperature dependent nor even narrowly defined (see Table II). At most temperatures, the best fit Θ was 45° ± 5°, although angles as low as 30° and, at low temperatures, angles as high as 75° could produce reasonable fits. As shown in Eq. (4), the anisotropic decay τ_D depends on Θ that has the jump time, τ_{ex}. These two parameters play off against each other to some extent. The results demonstrate that the jump angle is large and the overall best value is ~45°. The 45° ± 5° jump angle is within error of the 50° ± 5° jump angle that was observed in the water/ion jump exchange,[7,8] which suggests that this might be a common feature of H-bonding systems.

C. Thermodynamics of the slow exchange and SSD dynamics

In both the exchange times and the SSDs, the slow dynamics were found to be highly temperature dependent. The three corresponding time constants, the slow exchange time, and the slow components of the structural spectral diffusion for the HB and NB species are shown as an Arrhenius plot in Fig. 10 ($\tau_{ex,slow}$ for the slow exchange time in Table II, $t_{2,HB}$ in Table III, and $t_{2,NB}$ in Table IV for the SSDs). Within error, $t_{2,HB}$ is slightly faster than $\tau_{ex,slow}$, which are both almost an order of magnitude faster than $t_{2,NB}$, although $t_{2,NB}$ has the largest error bars because it is the smaller component in the line shape and is slower than both the exchange rate and (at low temperatures) the experimental window set by the vibrational lifetimes. All three sets of slow dynamics exhibit approximately the same Arrhenius behavior as well. The activation energy of $\tau_{ex,slow}$ is 41 ± 2 kJ/mol, that of $t_{2,HB}$ is 41 ± 6 kJ/mol, and that of $t_{2,NB}$ is 57 ± 18 kJ/mol. Within error, all three times have the same activation energy. The solid lines are the best linear fits. The black dashed line through the $t_{2,NB}$ data has the same slope as the blue and red lines.

The observed Arrhenius behavior is clearly different from the results of temperature dependent 2D IR experiments on analogous non-H-bonding liquids[38] and from dynamics studies of other fragile glass forming liquids.[31,32] In these liquids, the slow α-relaxation characteristically makes a transition from a purely Arrhenius temperature dependence at high temperatures to a steeper, super-Arrhenius, temperature dependence at low temperatures.[22,23] Previous studies of 2BPM with optical Kerr effect (OKE) spectroscopy demonstrated that its alpha relaxation over a similar temperature range had power law behavior, as predicted by Mode Coupling Theory (MCT).[32] This power law is reproduced in Fig. 10. While the power law describes the high temperature data as well as the

TABLE III. Structural spectral diffusion fit parameters of H-bonded PhSeCN in 2BPM. Frequency amplitudes, Δ_i; spectral diffusion time scales, t_i; and dephasing time, T_2, as defined in Eq. (2).

T (K)	Δ_1 (cm^{-1})	log[t_1/ps]	Δ_2 (cm^{-1})	log[t_2/ps]	T_2 (ps)[a]
355	2.0 ± 0.4	0.5 ± 0.2	2.2 ± 0.4	1.0 ± 0.3	1.8
345	1.7 ± 0.4	0.6 ± 0.2	2.4 ± 0.3	1.5 ± 0.4	1.8
335	1.5 ± 0.4	0.7 ± 0.2	3.1 ± 0.2	2.1 ± 0.4	1.9
325	2.2 ± 0.5	0.6 ± 0.2	3.5 ± 0.3	1.9 ± 0.4	2.2
315	2.3 ± 0.7	0.7 ± 0.3	3.7 ± 0.5	1.9 ± 0.3	2.3
300	2.7 ± 0.8	0.6 ± 0.2	3.9 ± 0.6	2.2 ± 0.4	2.5
290	2.4 ± 0.8	0.8 ± 0.3	4.4 ± 0.4	2.4 ± 0.5	2.6
280	1.7 ± 0.3	0.6 ± 0.2	5.1 ± 0.1	2.8 ± 0.2	3.0
270	1.5 ± 0.4	1.3 ± 0.3	5.4 ± 0.1	3.4 ± 0.3	3.2

[a]Determined from the fit of envelope of τ interferogram at $T_w = 0$. See the supplementary material.

Published under license by AIP Publishing

TABLE IV. Structural spectral diffusion fit parameters of non-H-bonded PhSeCN in 2BPM. Frequency amplitudes, Δ_i; spectral diffusion time scales, t_i; and dephasing time, T_2, as defined in Eq. (2).

T (K)	Δ_1 (cm^{-1})	log[t_1/ps]	Δ_2 (cm^{-1})	log[t_2/ps]	T_2[a] (ps)
355	1.8 ± 0.4	1.0 ± 0.4	3.0 ± 0.3	2.5 ± 0.7	2.8
345	1.7 ± 0.5	1.0 ± 0.4	3.0 ± 0.3	2.4 ± 0.4	3.0
335	1.7 ± 0.5	1.0 ± 0.3	3.0 ± 0.3	3.0 ± 0.7	3.5
325	1.8 ± 0.4	1.2 ± 0.5	3.0 ± 0.3	3.1 ± 0.8	3.4
315	2.0 ± 0.4	1.1 ± 0.6	2.8 ± 0.3	3.1 ± 1.2	3.6
300	1.8 ± 0.4	1.3 ± 0.5	3.0 ± 0.2	4.1 ± 1.2	4.4
290	1.5 ± 0.4	1.3 ± 0.5	3.1 ± 0.2	4.3 ± 1.5	4.2
280	1.6 ± 0.4	1.5 ± 0.7	3.1 ± 0.2	4.5 ± 1.0	5.5
270	1.4 ± 0.3	1.4 ± 0.7	3.2 ± 0.1	5.0 ± 1.5	5.6

[a]Estimated from dephasing times reported for PhSeCN in other glass formers. See the supplementary material.

Arrhenius fit does, there is no indication of the dynamical transition that has been measured previously in 2BPM by OKE. It remains possible that this super-Arrhenius behavior would be seen nearer the glass transition if sufficiently long time scales could be probed.

D. Fast exchange and SSD dynamics

The fast exchange and SSD dynamics display a similar trend as the slow dynamics, with the ~5 ps SSD of the HB population ($t_{1,HB}$ in Table III) being substantially faster than the ~10 ps dynamics of the fast exchange time ($\tau_{ex,fast}$ in Table II). $\tau_{ex,fast}$ was in turn slightly faster than the 10-15 ps SSD of the NB population ($t_{1,NB}$ in Table IV). Compared to the slower dynamics, the fast dynamics have a very mild temperature dependence, with the exchange time scale $\tau_{ex,fast}$ having an activation energy of 5.7 ± 4.6 kJ/mol. The SSD time constants have this same value within error. The activation energy is within error of the fast SSD in non-H-bonding liquids, 3 and 4 kJ/mol for both OTP and BZP.[37,38] The fast SSD in 2BPM may be identical in behavior to the fast spectral diffusion seen in these other liquids, which would result in the same mild temperature dependence that was more readily determined from the non-H-bonding liquids. It was previously seen in OTP that the same mild temperature dependence of fast spectral diffusion dynamics persisted deep into the glass phase,[37] and it is likely that these fast dynamics would behave similarly.

As was described in Sec. IV A, the fraction f of molecules undergoing fast exchange drops monotonically with decreasing temperature, from about 80% at 355 K to 15% at 270 K. The frequency amplitudes [Δ_i in Eq. (2); the standard deviation of the range of frequencies sampled with a particular time constant] of the fast spectral diffusion undergo a similar decrease, although the effect is comparably mild. The amplitude associated with the fast dynamics in the HB population, which decreases more unambiguously than the NB population, goes from ~50% of the decay at 355 K to 7% at 270 K (see Table III). There are two plausible mechanisms for this reduced effect in the SSD relative to the orientational relaxation, where the fast and slow motions are assumed to be mechanically similar. The first is that SSD depends on both the orientational and density fluctuations of the surrounding material.[37,38] It is then possible that the slower density fluctuations in the material are more significant for SSD (strong coupling) than the faster density fluctuations. The second is that the ratios of orientational motion are for the PhSeCN probe and not the 2BPM solvent: it is possible that the ratio of mobile 2BPM molecules is different from that of the PhSeCN molecules. These two mechanisms are not mutually exclusive and both may impact the measurements.

E. The physicality of the two heterogeneous exchange models

While the two models of heterogeneous exchange illustrated in Fig. 9 give virtually identical fits to the experimental data, we can also use the thermodynamic data described in Secs. IV C and IV D to evaluate the reasonableness of each model. It was seen that the effective slow exchange and the fraction of molecules exhibiting slow exchange have steep temperature dependences, while the fast exchange dynamics have very modest temperature dependences. Additionally, the jump angle of exchange must be at least comparable for both time scales to be consistent with observations.

These facts can be explained well with the dynamical interconversion model (model 2 in Figs. 9). The liquid structures that comprise the fast subensemble are then a higher energy, configurational transition state that must be accessed before exchange can occur. Once in this high-energy state, exchange can happen readily with only a small energy barrier. Because exchange only happens for these transition state configurations, all of the jump angles will be essentially the same. Model 2 in Fig. 9 eliminates the necessity for explaining why the slow ensemble exhibits the same jump angle as the fast ensemble (model 1 in Fig. 9). If the slow exchange occurred, it would be slow because of differences in the liquid structures from the fast exchanging structures. It is physically reasonable to postulate that the structural differences that would give rise to much slower exchange are unlikely to result in identical jump angles. The model 2 interconversion scenario similarly eliminates the issue of having extremely different thermodynamics for what is essentially the same physical event in the fast and slow subensembles in the model 1 persistent dynamics scenario. While the two models cannot be experimentally distinguished, the model 2 dynamical interconversion scenario provides a more reasonable physical interpretation that avoids the awkward arguments that would be needed to use the model 1 scenario with persistent dynamical subensembles.

The above arguments, which give substantial support for the model 2 dynamical interconversion scenario, lead to a very important conclusion. The "slow exchange times" in the measurements are actually the time for interconversion from the slow dynamical subensemble to the fast dynamical subensemble. This transition must be mediated by structural evolution in the liquid itself. Then the $\tau_{ex,slow}$ in Table II are the temperature dependent times for the structural changes that convert slow domains to fast domains in the 2BPM supercooled liquid. The slow to fast domain interconversion times range from 40 ps at 355 K to 5000 ps at 270 K.

V. CONCLUSIONS

2D IR spectroscopy on the H-bonding glass forming liquid 2BPM demonstrated polarization-dependent effects that were far in

Published under license by AIP Publishing

excess of what has been observed in similar non-H-bonding liquids or what has been predicted by standard theory of reorientation-induced spectral diffusion. This anomaly was resolved through the observation of two separate but spectrally overlapped populations of the PhSeCN probe molecules in the linear FT-IR spectra and isotropic pump-probe decays: H-bonded and non-H-bonded populations. The observed polarization dependence of the spectral diffusion arises due to chemical exchange between these two populations. The observation of exchange-induced spectral diffusion demonstrates the importance of taking polarization dependent 2D spectra when there are potentially strong, directional interactions present in a system, e.g., hydrogen bonds.

By adapting prior treatments of chemical exchange associated with large "jump" angles,[7] a kinetic model was developed that was capable of describing the large polarization dependence in the 2D IR decays. Furthermore, the results demonstrate how 2D IR line shape analyses can be used to extract information on chemical exchange even when the component linear IR absorption bands are not spectrally separated. The experiments and analysis produced a number of significant results. First, to describe the magnitude of the 2D IR polarization differences at long times, chemical exchange had to account for the orientational motion of the PhSeCN molecules through large angle jumps (~45°) in exchanging between H-bonding and non-H-bonding subensembles. Second, to describe the magnitude of the polarization difference at short times, the nonexponential nature of the pump-probe anisotropy arose from heterogeneous orientational dynamics (and thus heterogeneous exchange behavior), as opposed to confined angle, "wobbling" motions that are commonly invoked to explain non-exponential orientational relaxation.[54,55] To the best of the authors' knowledge, this is the first experimental evidence of heterogeneity in orientational motion in glass forming liquids on these time scales and temperature ranges.

The temperature dependence of the 2BPM data showed that, while heterogeneity is present at all temperatures studied, the liquid becomes very heterogeneous at mild supercooling, with significant populations exchanging on picosecond and nanosecond time scales. Furthermore, the associated SSD decays of both the H-bonded and non-H-bonded species were found to have the same activation energies as the exchange dynamics. No super-Arrhenius temperature dependence, that is typical of "fragile" glass forming liquids, was observed.

In the data analysis using heterogeneous kinetics, it was found that two models could describe the data with equal efficacy. These are depicted in Fig. 9. In pathway 1, the liquid has regions of slow jump orientational relaxation and regions of fast jump orientational relaxation. There is no interconversion between slow and fast regions on the experimental time scale. In pathway 2, orientational relaxation in the slow regions is so slow that it is not observed on the experimental time scale. Rather, what is manifested as the slow jump orientational relaxation is the interconversion of slow domains into fast domains. The interconversion is slow but is followed by a fast jump, appearing in the data as a slow jump component. The experimental observations, including temperature dependence, jump angles, activation energies, the kinetic modeling, and physical arguments, lead to the conclusion that pathway 2 is correct. Therefore, the slow exchange time, $\tau_{ex,slow}$, is actually the interconversion time from liquid domains that have slow dynamics to liquid domains that have fast dynamics. The temperature dependent values of the domain interconversion times ($\tau_{ex,slow}$) are given in Table II. The times range from 40 ps at 355 K to 5000 ps at 270 K.

SUPPLEMENTARY MATERIAL

See supplementary material for S1: jump exchange kinetic model; S2: determining the line shape parameters; S3: calculating the XISD line shapes; S4: implementing the homogeneous "wobbling" model; S5: implementing the heterogeneous orientational relaxation/chemical exchange; S6: fit method details; S7: additional notes on temperature dependent parameters; and S8: plots of homogeneous and heterogeneous model fits at all temperatures.

ACKNOWLEDGMENTS

This work (D.J.H., S.M.F.-C., and M.D.F.) was supported by the Office of Naval Research under a Multidisciplinary University Research Initiative (Contract No. N00014-17-1-2656). Additional support for the instrumentation and M.D.F. was provided by the Division of Chemical Sciences, Geosciences, and Biosciences, Office of Basic Energy Sciences of the U.S. Department of Energy through Grant No. DE-FG03-84ER13251.

REFERENCES

[1] H.-S. Tan, I. R. Piletic, and M. D. Fayer, J. Opt. Soc. Am. B **22**, 2009–2017 (2005).
[2] Y. L. A. Rezus and H. J. Bakker, J. Chem. Phys. **123**, 114502 (2005).
[3] M. Cho, G. R. Fleming, and S. Mukamel, J. Chem. Phys. **98**, 5314–5326 (1993).
[4] S. Mukamel, *Principles of Nonlinear Optical Spectroscopy* (Oxford University Press, New York, 1995).
[5] O. Golonzka and A. Tokmakoff, J. Chem. Phys. **115**, 297–309 (2001).
[6] R. M. Hochstrasser, Chem. Phys. **266**, 273–284 (2001).
[7] M. Ji and K. J. Gaffney, J. Chem. Phys. **134**, 044516 (2011).
[8] M. Ji, M. Odelius, and K. J. Gaffney, Science **328**, 1003–1005 (2010).
[9] M. T. Zanni, N.-H. Ge, Y. S. Kim, and R. M. Hochstrasser, Proc. Natl. Acad. Sci. U. S. A. **98**, 11265–11270 (2001).
[10] S. Woutersen and P. Hamm, J. Phys. Chem. B **104**, 11316–11320 (2000).
[11] P. L. Kramer, J. Nishida, and M. D. Fayer, J. Chem. Phys. **143**, 124505 (2015).
[12] P. L. Kramer, J. Nishida, C. H. Giammanco, A. Tamimi, and M. D. Fayer, J. Chem. Phys. **142**, 184505 (2015).
[13] C. H. Giammanco, P. L. Kramer, S. A. Yamada, J. Nishida, A. Tamimi, and M. D. Fayer, J. Chem. Phys. **144**, 104506 (2016).
[14] Z. Ren and S. Garrett-Roe, J. Chem. Phys. **147**, 144504 (2017).
[15] S. Mukamel, Annu. Rev. Phys. Chem. **51**, 691–729 (2000).
[16] S. Park, K. Kwak, and M. D. Fayer, Laser Phys. Lett. **4**, 704–718 (2007).
[17] P. Hamm and M. Zanni, *Concepts and Methods of 2D Infrared Spectroscopy* (Cambridge University Press, 2011).
[18] Z. Ren, J. Kelly, C. P. Gunathilaka, T. Brinzer, S. Dutta, C. A. Johnson, S. Mitra, and S. Garrett-Roe, Phys. Chem. Chem. Phys. **19**, 32526–32535 (2017).
[19] S. A. Yamada, W. H. Thompson, and M. D. Fayer, J. Chem. Phys. **146**, 234501 (2017).
[20] R. Yuan, C. Yan, and M. Fayer, J. Phys. Chem. B **122**, 10582–10592 (2018).
[21] D. Zhou, Q. Wei, S. Wang, X. Li, and H. Bian, J. Phys. Chem. Lett. **10**, 176 (2018).
[22] C. A. Angell, K. L. Ngai, G. B. McKenna, P. F. McMillan, and S. W. Martin, J. Appl. Phys. **88**, 3113–3157 (2000).
[23] P. G. Debenedetti and F. H. Stillinger, Nature **410**, 259–267 (2001).
[24] M. D. Ediger, C. A. Angell, and S. R. Nagel, J. Phys. Chem. **100**, 13200–13212 (1996).

Published under license by AIP Publishing

[25]M. T. Cicerone, Q. Zhong, and M. Tyagi, Phys. Rev. Lett. **113**, 117801 (2014).
[26]J. Jang and D. K. Lee, Polymer **44**, 8139–8146 (2003).
[27]A. E. Zachariades and R. S. Porter, J. Appl. Polym. Sci. **24**, 1371–1382 (1979).
[28]L.-T. Lim, I. J. Britt, and M. A. Tung, J. Appl. Polym. Sci. **71**, 197–206 (1999).
[29]M. G. A. Vieira, M. A. Da Silva, L. O. Dos Santos, and M. M. Beppu, Eur. Polym. J. **47**, 254–263 (2011).
[30]H. M. Park, M. Misra, L. T. Drzal, and A. K. Mohanty, Biomacromolecules **5**, 2281–2288 (2004).
[31]H. Cang, V. N. Novikov, and M. D. Fayer, Phys. Rev. Lett. **90**, 197401 (2003).
[32]H. Cang, V. N. Novikov, and M. D. Fayer, J. Chem. Phys. **118**, 2800 (2003).
[33]J. Baran, N. A. Davydova, and M. Drozd, J. Mol. Liq. **127**, 109–112 (2006).
[34]N. Davydova, J. Baran, and M. Drozd, J. Non-Cryst. Solids **353**, 1793–1797 (2007).
[35]J. Baran, N. A. Davydova, V. I. Melnik, and V. P. Vorob'ev, J. Mol. Liq. **153**, 174–177 (2010).
[36]J. Baran, N. A. Davydova, M. Drozd, and A. Pietraszko, J. Phys.: Condens. Matter **18**, 5695–5702 (2006).
[37]D. J. Hoffman and M. D. Fayer, J. Phys. Chem. B **121**, 10417–10428 (2017).
[38]D. J. Hoffman, K. P. Sokolowsky, and M. D. Fayer, J. Chem. Phys. **146**(12), 124505 (2017).
[39]H. Bian, J. Li, X. Wen, and J. Zheng, J. Chem. Phys. **132**, 184505 (2010).
[40]J. C. Owrutsky, D. Raftery, and R. M. Hochstrasser, Annu. Rev. Phys. Chem. **45**, 519–555 (1994).
[41]L. J. G. W. Van Wilderen, D. Kern-Michler, H. M. Müller-Werkmeister, and J. Bredenbeck, Phys. Chem. Chem. Phys. **16**, 19643–19653 (2014).
[42]B. Błasiak, A. W. Ritchie, L. J. Webb, and M. Cho, Phys. Chem. Chem. Phys. **18**, 18094–18111 (2016).
[43]S. Bagchi, S. D. Fried, and S. G. Boxer, J. Am. Chem. Soc. **134**, 10373–10376 (2012).
[44]J. Zheng, K. Kwak, and M. D. Fayer, Acc. Chem. Res. **40**, 75–83 (2007).
[45]A. Tokmakoff, J. Chem. Phys. **105**, 1–12 (1996).
[46]P. L. Kramer, C. H. Giammanco, A. Tamimi, D. J. Hoffman, K. P. Sokolowsky, and M. D. Fayer, J. Opt. Soc. Am. B **33**, 1143 (2016).
[47]K. Kwak, D. E. Rosenfeld, and M. D. Fayer, J. Chem. Phys. **128**(20), 204505 (2008).
[48]K. Kwak, S. Park, I. J. Finkelstein, and M. D. Fayer, J. Chem. Phys. **127**(12), 124503 (2007).
[49]R. Kubo, in *Fluctuation, Relaxation, and Resonance in Magnetic Systems*, edited by D. Ter Haar (Oliver & Boyd, London, 1961).
[50]K. Kwak, J. Zheng, H. Cang, and M. D. Fayer, J. Phys. Chem. B **110**, 19998–20013 (2006).
[51]Y. S. Kim and R. M. Hochstrasser, J. Phys. Chem. B **113**(24), 8231–8251 (2009).
[52]J. Zheng, K. Kwak, J. B. Asbury, X. Chen, I. R. Piletic, and M. Fayer, Science **309**, 1338–1343 (2005).
[53]R. Richert, J. Phys.: Condens. Matter **14**, R703–R738 (2002).
[54]G. Lipari and A. Szabo, Biophys. J. **30**, 489–506 (1980).
[55]G. Lipari and A. Szabo, J. Am. Chem. Soc. **104**, 4546–4559 (1982).
[56]D. E. Moilanen, E. E. Fenn, Y.-S. Lin, J. L. Skinner, B. Bagchi, and M. D. Fayer, Proc. Natl. Acad. Sci. U. S. A. **105**, 5295–5300 (2008).
[57]F. H. Stillinger and P. G. Debenedetti, Annu. Rev. Condens. Matter Phys. **4**, 263–285 (2013).
[58]I. Chang and H. Sillescu, J. Phys. Chem. B **101**, 8794–8801 (1997).
[59]L. Berthier and J. P. Garrahan, Phys. Rev. E **68**, 041201 (2003).
[60]M. D. Ediger and P. Harrowell, J. Chem. Phys. **137**, 080901 (2012).
[61]T. G. Lombardo, P. G. Debenedetti, and F. H. Stillinger, J. Chem. Phys. **125**, 174507 (2006).
[62]L. J. Lewis and G. Wahnström, Phys. Rev. E **50**, 3865–3877 (1994).
[63]J. Qian, R. Hentschke, and A. Heuer, J. Chem. Phys. **110**, 4514–4522 (1999).
[64]S. Kämmerer, W. Kob, and R. Schilling, Phys. Rev. E **56**, 5450–5461 (1997).
[65]S. Sastry, P. G. Debenedetti, and F. H. Stillinger, Nature **393**, 554–557 (1998).
[66]Y. Brumer and D. R. Reichman, Phys. Rev. E **69**, 041202 (2004).
[67]F. Mallamace, C. Branca, C. Corsaro, N. Leone, J. Spooren, S.-H. Chen, and H. E. Stanley, Proc. Natl. Acad. Sci. U. S. A. **107**, 22457–22462 (2010).

Published under license by AIP Publishing